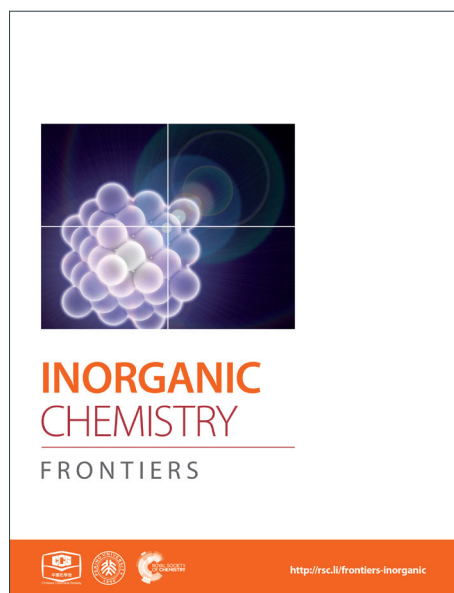
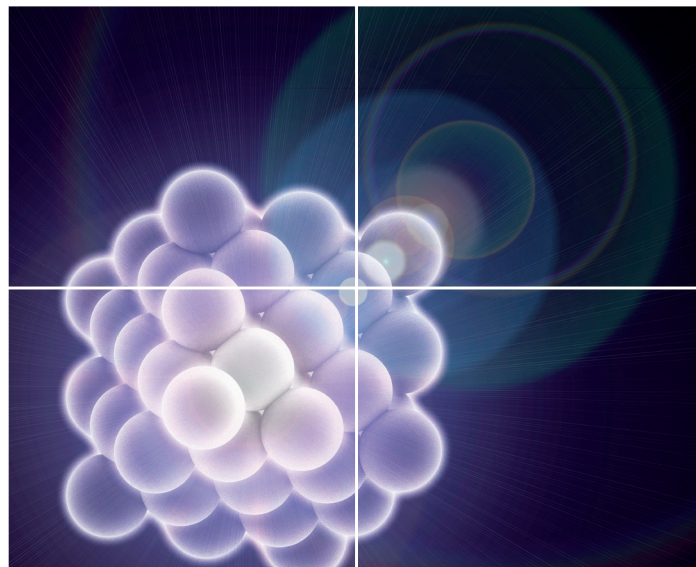


INORGANIC CHEMISTRY

FRONTIERS

Accepted Manuscript



This is an *Accepted Manuscript*, which has been through the Royal Society of Chemistry peer review process and has been accepted for publication.

Accepted Manuscripts are published online shortly after acceptance, before technical editing, formatting and proof reading. Using this free service, authors can make their results available to the community, in citable form, before we publish the edited article. We will replace this *Accepted Manuscript* with the edited and formatted *Advance Article* as soon as it is available.

You can find more information about *Accepted Manuscripts* in the [Information for Authors](#).

Please note that technical editing may introduce minor changes to the text and/or graphics, which may alter content. The journal's standard [Terms & Conditions](#) and the [Ethical guidelines](#) still apply. In no event shall the Royal Society of Chemistry be held responsible for any errors or omissions in this *Accepted Manuscript* or any consequences arising from the use of any information it contains.

Cite this: DOI: 10.1039/c0xx00000x

www.rsc.org/xxxxxx

ARTICLE TYPE

Experimental, DFT and Quantum Monte Carlo Studies of A Series of Peptide-based Metal-Organic Frameworks: Synthesis, Structures and Properties

Gui-lin Zhuang,^a Li Tan,^a Wu-lin Chen,^{ac} Jun Zheng,^b Hong-zhou Yao,^a Xing Zhong,^a Jian-guo Wang^{*a}⁵ Received (in XXX, XXX) Xth XXXXXXXXXX 20XX, Accepted Xth XXXXXXXXXX 20XX

DOI: 10.1039/b000000x

A series of bio-analogous peptide-based metal-organic frameworks (Mn (**1**), Fe (**2**), Co (**3**), Cu (**4**), Ag (**5**) and Pb (**6**)) based on one cyclic dipeptide (2, 5-piperazinedione-1, 4-diacetic acid, H₂PODC) were obtained and the relation between properties (Luminescence and Magnetism) and structure were investigated. Crystal structure analysis show that: (1) **1-3** feature three-dimensional isomorphous framework; (2) **4** shows one two-dimensional plane structure; (3) **5** shows three-dimensional framework with one alternate Ag-Ag chain ($d_{\text{Ag-Ag}} = 2.7918$ and 2.9346 Å); (4) **6** indicates three-dimensional structure with one dimensional 7.0×7.0 Å² channel. Combination of magnetic measures and Quantum Monte Carlo (QMC) studies reveals **1** has anti-ferromagnetic property with J of -0.5 cm⁻¹ and **4** exhibit ferromagnetic property with J of 2.23 cm⁻¹, while both **2** and **3** show ferrimagnetic property. Spin polarized density functional theory (DFT) calculations uncover that antiferromagnetism of **1** is attributed to the coupling of paramagnetic Mn(II) ions by $-/+$ spin nets of linking carboxylate, while in **4** ferromagnetic superexchange of Cu(II) ions is derived from spin polarization effect through carboxylate bridge in the $+/+$ spin nets of linking carboxylates. Furthermore, DFT calculation results shows that two absorption peaks of **5** should be attributed to the transition of valence band (VB)→ the second empty bands and VB→conduction band (CB), and one emission peak is result from the transition of CB→VB, where the electrons transfer from Ag-Ag metal bond to localized $4d$ orbits of Ag atoms.

20 Introduction

In the last two decades, Metal-organic Frameworks (MOFs) or coordination polymers are of contemporary interest, not merely due to aesthetically interesting structures¹ by the amalgamation of chemistry and geometry, but mainly due to potential applications in adsorption², separation³, catalysis⁴, luminescence⁵, magnetism⁶ and nonlinear optics⁷. The design philosophy of Second Building Unit (SBU)⁸ provides a large promotion to the assembly of MOFs, where the linkers involve in polycarboxylic acid (e. g. aromatic carboxylic acid and fatty acid)⁹, imidazole¹⁰ and N-O mixed ligands¹¹. Arguably most notable in this context is the research on bio-analogous MOFs from biologically derived molecules (e. g. amino acids and nucleobases¹²). That may be attributed to two aspects: (1) potential application of a next generation of biomimetic porous materials; (2) investigation of interaction between biological groups and trace metal ions. Peptide, as a well-known biological molecule, always plays an important role in molecular biology, such as antibody, protein tags. Moreover, unique functional groups (e. g. carboxylate and amino group) and flexibility of peptide endow them with an adaptable-porous linker of MOFs. Since the pioneer work of Taubert et. al.¹³, these studies concerning the synthesis and properties of peptide-based MOFs have begun to be emerging¹⁴. For instance, Rosseinsky et. al. have reported two peptide-based adaptable porous materials: [Zn(Gly-Ala)₂]^{14a} and [Zn(Gly-Thr)₂]^{14b}. However, owing to congenital friability of peptide bond, designable synthesis of peptide-based MOFs have still been a challenge object.

Moreover, accurate design of material relies on the information

regarding connection between structure and property. Therefore, investigations of the structure-to-function relationship have been an important and challenging topic in the field of MOFs. In this regard, experimental views alone are hard to produce the profound comprehensions. Currently, combination of theoretical calculations and experimental studies has become to be an effective tool. Varies theoretical simulation methods, including DFT¹⁵, Monte Carlo (MC)¹⁶, and molecular dynamics (MD)¹⁷, have been widely applied to forecast or explain interesting experimental phenomenon of MOFs. However, to the best of our knowledge, corresponding studies regarding the structure-to-function relationship of peptide-based MOFs have been never reported.

In this article, we report the synthesis and structure of a series of new peptide-based MOFs, and focus on magnetic and luminescence properties. Furthermore, via QMC and DFT calculations, we further investigated the relations of magnetism-structure and luminescence-structure.

Result and Discussion

Crystal structure description

Compound **1**, [Mn(PODC)(H₂O)₂], crystallized in $P2(1)/c$ space group of monoclinic system. Single-crystal X-Ray diffraction analysis reveals that the asymmetric unit contains half Mn(II) ion, half PODC²⁻ ligand and one aqua ligand. As shown in Fig. 1(a), the coordination environment of Mn(II) ion can be viewed as a distorted octahedron, featuring the contributions by four carboxylate oxygen from PODC²⁻ ligands and two aqua

Cite this: DOI: 10.1039/c0xx00000x

www.rsc.org/xxxxxx

ARTICLE TYPE

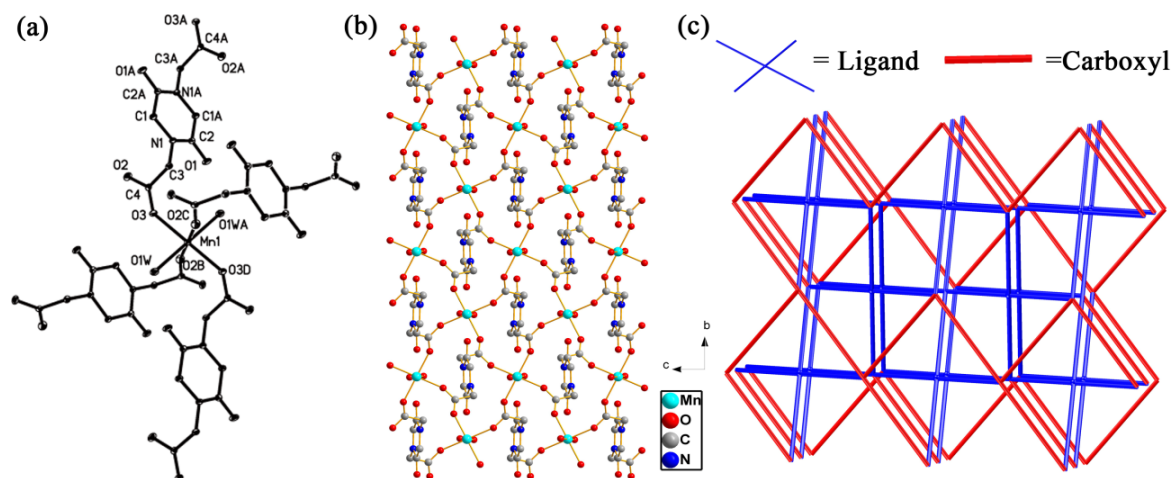


Fig. 1 (a) ORTEP plot showing coordination environment of Mn(II) ions; two-dimensional structure of **1** viewed along a axis (b) and topology sketch map of **1** (c).

ligands. The coordination mode of PODC^{2-} is shown in Fig. S3(a). The corresponding bond lengths of Mn–O are 2.1407–2.2122 Å, consistent with the previous results¹⁸. Inspecting the whole structure of **1**, it is observed that through the *syn-anti* carboxylate bridges, each Mn(II) ion connects with adjacent ones so as to form two-dimensional $\{\text{Mn}(\text{COO})_n\}$ planes structure (see Fig. 1(b)), where the distance of Mn···Mn and the torsion angle of Mn–O–C–O–Mn are 6.102 Å and 119.48°, respectively. Furthermore, the 2D $\{\text{Mn}(\text{COO})_n\}$ plane bridges with adjacent ones via PODC^{2-} ligands, leading to a three-dimensional framework, as shown in Fig. 1(c). The short Schläfli vertex notation of the net can be represented as $\{6^5.8\}$, as indicated by the TOPOS software¹⁹.

Moreover, both **2** and **3** exhibit three-dimensional frameworks with **1**. The bond lengths of Fe(II)–O and Co(II)–O are 2.0689(11)–2.1501(13) and 2.0739(10)–2.1095(12) Å. Additionally, the distance of Fe···Fe and Co···Co are 6.028 and 6.025 Å. Generally, these bond distances are slightly smaller than that of **1**.

Different from compound **1-3**, crystal structure analysis reveals that compound **4** displays two-dimensional plane structure with the space group of $C2/c$. As is clear from Fig.2(a), the asymmetric unit of **4** consists of half Cu(II) ion, half PODC^{2-} ligand and one aqua ligand. Like those of **1-3**, the coordination configuration of Cu(II) ion can be described as a distorted octahedron, featuring the coordination by four carboxylate oxygen from PODC^{2-} ligands and two aqua ligands. The resulting bond lengths of Cu–O are 1.9501(14)–1.9573(15) Å, within the expected range reported for Cu(II)–based compounds.²⁰ PODC^{2-} ligand exhibits the same coordination mode as these of **1**. Via *syn-anti* carboxylate bridges, each Cu(II) ion connects with neighboring ones, resulting in 1D $\{\text{Cu}(\text{COO})_n\}$ chains. Furthermore, each chain is linked to adjacent ones by PODC^{2-} ligands so as to generate 4⁴-net 2D plane structure, as displayed in Fig. 2(b). The 3D supramolecular architecture can be seen as

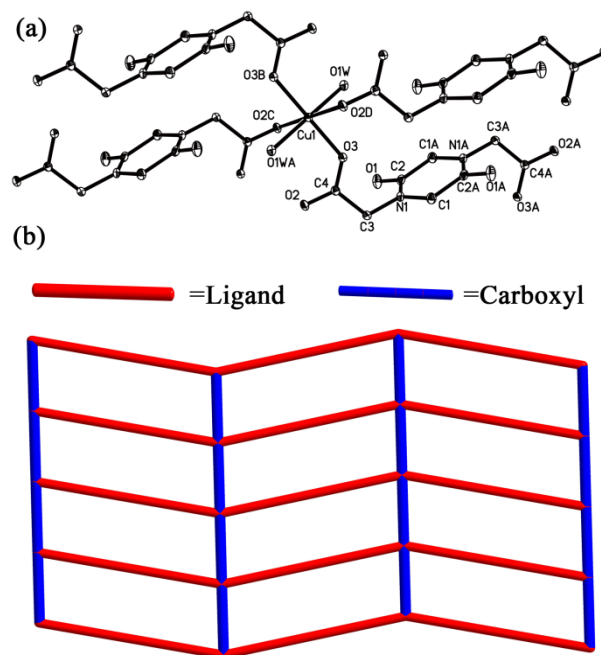


Fig. 2 (a) ORTEP plot showing coordination environment of Cu(II) ions; (b) two-dimensional topology sketch map of compound **4** viewed along a axis.

the 2D layers linked by weak interaction force, e.g. Van der Waals' force.

Compound **5** crystallized in monoclinic system with $P2(1)/n$ space group. Analysis of the single-crystal diffraction data indicates that the asymmetric unit of **5** contains one Ag(I) ion and half PODC^{2-} ligand. As shown in Fig. 3(a), the Ag(I) ion is quad-coordinated tetrahedron with two carboxylate O atoms and two carbonyl O atoms from four PODC^{2-} ligands. The corresponding bond length of Ag–O bond are 2.184(4)–2.8003(39) Å, being in agreement with those of quad-coordinated Ag(I)²¹. Interestingly,

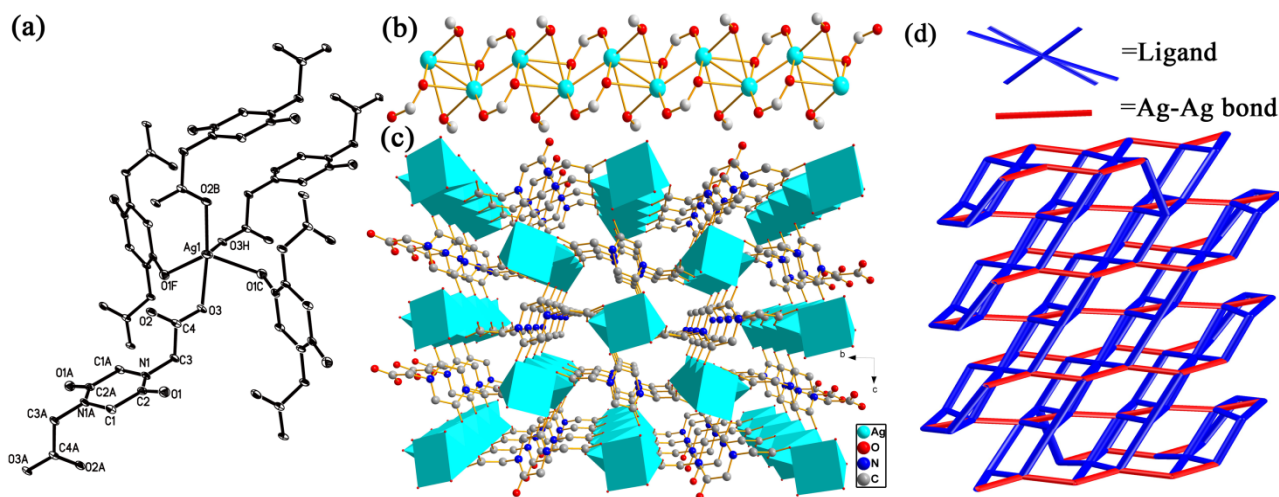


Fig. 3 (a) ORTEP plot showing coordination environment of Ag(I) ions in **5**; (b) $\{\text{AgO}(\text{COO})\}_n$ chain along a axis; three-dimensional supramolecule architecture polyhedron (c) view and topology sketch map (d) of compound **5** along a axis.

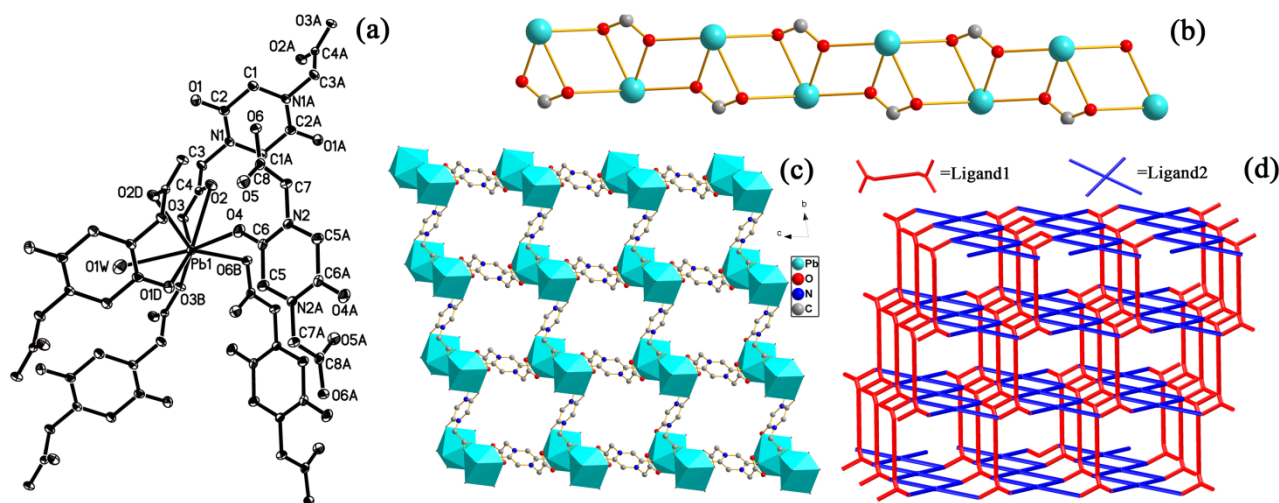


Fig. 4 (a) ORTEP plot showing coordination environment of Pb(II) ions in **6**; (b) $\{\text{Pb}(\text{COO})\}_n$ chain along a axis; three-dimensional supramolecule architecture polyhedron (c) and topology sketch map (d) of compound **6** along a axis.

PODC²⁻ ligand exhibits a different coordination mode from those of **1-4**, where both carboxylate and carbonyl oxygen atoms participate in coordinating to Ag(I) ions, as shown in Fig. S3(b). Each Ag(I) ion connects with another Ag(I) ion via two carbonyl oxygen atoms and one μ^2 : η^1 , η^2 -carboxylate to generate $\{\text{Ag}_2\}$ unit, as shown in Fig. 3(b). Along *a* axis, connection of two adjacent ones through two μ^2 : η^1 , η^2 -carboxylates results in a 1D $\{\text{AgO}(\text{COO})\}_n$ chain, which further form 3D structure by use of two opposite carboxylates and carbonyls of PODC²⁻ ligand, as displayed in Fig.3(c-d). The short Schläfli vertex notation of the net can be described as $\{4^{14}.6\}^2\{4^{44}.6^{22}\}$, as calculated by the TOPOS software¹⁹. It must be mentioned that two different Ag—Ag metal bond ($d_{\text{Ag-Ag}} = 2.7918$ and 2.9346 Å) appears in **5**.

The single-crystal X-Ray diffraction analysis shows that compound **6** crystallized in triclinic symmetry with the space group of *P*-1. In the asymmetric unit, there are one crystallographically independent Pb(II) ion, one PODC²⁻ ligand, one aqua ligand and four guest water molecules. As shown in Fig. 4(a), the coordination environment of Pb(II) ion features the contributions of six carboxylate oxygens, one carbonyl oxygen and one aqua ligands. The corresponding bond length of Pb—O

are $2.479(2)$ – $2.9557(45)$ Å, comparable to those in previous reported compounds²². In **6**, PODC²⁻ ligand exhibits two different coordination modes (see Fig. S3(c-d)). The 3D structure of **6** can be described as follows: (1) through the carboxylates, each Pb(II) ion connects with adjacent ones along *a* axis to form 1D $\{\text{Pb}(\text{COO})\}_n$ chain, as shown in Fig. 4(b); (2) each chain further links each other along *b* and *c* axis by use of two opposite carboxylates and carbonyl of PODC²⁻ ligand, as depicted in Fig. 4(c) and (d). The topology symbol is $\{4^4.6^2\}\{4^6.6^4\}^2\{4^8.6^6.8\}$, as indicated by the TOPOS software¹⁹. Notably, the channel of 7.0×7.0 Å² size along *a* axis was observed in **6**, as displayed in the space filling view of Fig. S4. Three guest water molecules in one unit-cell are enveloped in the channels. Interestingly, they display different dissociative temperature (see Fig. S5). Additionally, the pore volume calculated through the PLATON program is approximately 250.4 Å³ per unit cell volume (32.5%).

Magnetism-structure relation: Magnetic Properties, QMC Simulation and DFT calculation.

The magnetic properties of **1-3** are investigated through variable-temperature susceptibility measurements in the

temperature range of 2.0 to 300 K with an applied magnetic field of 1000 Oe. As shown in Fig. 5, the $\chi_m T$ value at room temperature (300 K) is $4.28 \text{ cm}^3 \text{ mol}^{-1} \text{ K}$ for **1**, consistent with the value of $4.38 \text{ cm}^3 \text{ mol}^{-1} \text{ K}$ for one independent Mn(II) ion ($g=2.0$). However, the $\chi_m T$ value at 300 K are 7.77 for **2** and $3.08 \text{ cm}^3 \text{ mol}^{-1} \text{ K}$ for **3** which are larger than those of one independent Fe(II) or Co(II) ion ($g=2.0$) expected by the Curie law²³. That may be due to contribution of orbital magnetic moment²⁴. As the temperature decreases, the value of $\chi_m T$ of **1** decreases slowly and reaches a value of $0.43 \text{ cm}^3 \text{ mol}^{-1} \text{ K}$ at 2 K. As shown in Fig. S6, the data of χ_m^{-1} vs T over the temperature range of 100–300 K fit well with the Curie-Weiss law²³ with Weiss constant $C=4.39 \text{ cm}^3 \text{ mol}^{-1} \text{ K}$ and Curie constant $\theta=-7.89 \text{ K}$, which reveals an overall very weak anti-ferromagnetic property. However, upon lowering of the temperature, the value of $\chi_m T$ of **2** and **3** decreases slowly and reaches a value of $2.66 \text{ cm}^3 \text{ mol}^{-1} \text{ K}$ for **2** and $2.07 \text{ cm}^3 \text{ mol}^{-1} \text{ K}$ for **3** at about 6 K. Subsequently, both of them increase abruptly and reach the maximum of $4.15 \text{ cm}^3 \text{ mol}^{-1} \text{ K}$ for **2** and $6.09 \text{ cm}^3 \text{ mol}^{-1} \text{ K}$ for **3** at 2 K. Generally, it is observed that both **2** and **3** exhibit ferrimagnetic behavior. Likewise, the fitting for χ_m^{-1} vs T over the temperature range of 100–300 K (see Fig. S6) also gives the best parameters: $C=8.90 \text{ cm}^3 \text{ mol}^{-1} \text{ K}$ and $\theta=-160.22 \text{ K}$ for **2**; $C=3.16 \text{ cm}^3 \text{ mol}^{-1} \text{ K}$ and $\theta=-8.07 \text{ K}$ for **3**, which exhibits that they feature anti-ferromagnetic properties at high temperature.

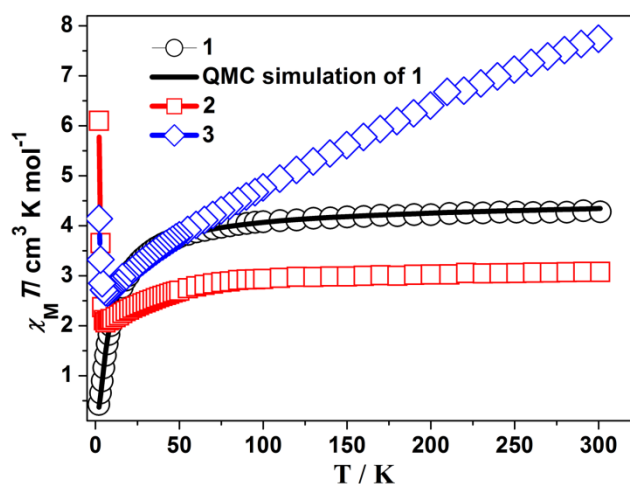


Fig.5 Experiment plot of $\chi_m T$ vs T of **1**(black \circ), **2**(red \square), **3**(blue \diamond); QMC fitting line (solid line) of **1**.

In order to identify the magnetic exchange interactions of **1**, the fitting to the plot of $\chi_m T$ vs T with the given model were performed. As displayed in Fig.S8(a) and (b), magnetic coupling of **1** can be attributed to the interaction between two Mn(II) ions. However, due to periodic characteristic, the fitting based on well-known Irreducible Tensor Operators method is impossible. Based on the Hamilton operator as shown in Fig.S8(c), therefore, we herein applied our QMC fitting program (See ESI), which invokes LOOP module of ALPS project²⁵. Coupling parameter J is utilized to describe the role of *syn-anti* carboxylate bridge between two adjacent Mn(II) ions. Weak interaction (zJ) constant²⁶, which has the capability of describing the interaction of the hydrogen bonds between two 2D layer frameworks, was also taken into account. According to the principle of least reliability factor R (see Fig. S8(d)), the obtained best parameters

are that: $J = -0.5 \text{ cm}^{-1}$, $zJ = -0.10 \text{ cm}^{-1}$, $g = 1.99$ and $R = 8.1 \times 10^{-5}$, where R is calculated from $\sum [(\chi_m T)_{\text{obs}} - (\chi_m T)_{\text{calcd}}]^2 / \sum [(\chi_m T)_{\text{obs}}]^2$. The little value (-0.50 cm^{-1}) of J reveals a weak antiferromagnetic propagation pathway of *syn-anti* carboxylate bridge. The zJ value of -0.10 cm^{-1} also displays a weak antiferromagnetic coupling between two layers, owing to the effect of weak-interaction (e.g. hydrogen bond). However, many attempts to simulate the magnetic susceptibility for **2** and **3** with the help of our fitting program were failed. Because six-coordinate Fe(II)/Co(II) ions usually present considerable first-order orbital momentum²⁴, the Hamiltonian operator must be supplemented by the orbitally dependent exchange interactions and spin-orbit coupling effects.

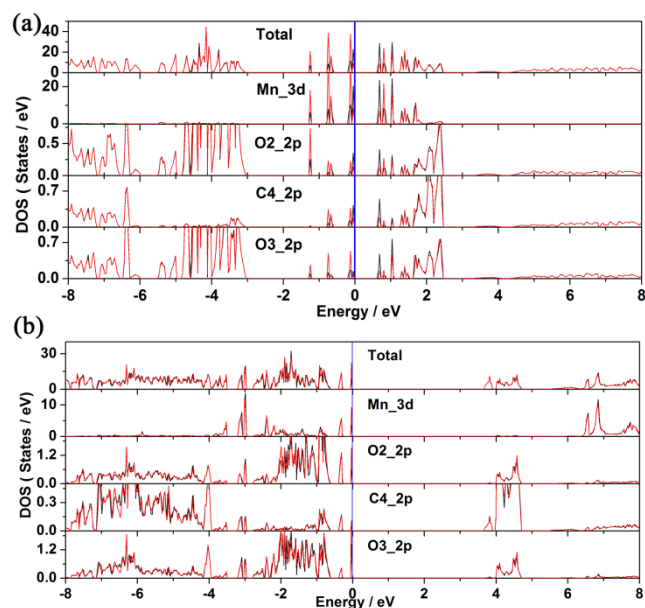


Fig. 6 PDOS of **1** under the U_{eff} of 0.0 eV (a) and 6.01 eV (b) in spin-up (black) and spin-down (red) with Fermi level (blue line).

Table 1 theoretical spin magnetic moments (μ_B) of **1**.

$U_{\text{eff}} / \text{eV}$	0.00	6.01
Mn1	1.063	4.720
Mn2	-1.067	-4.720
O2	-0.019	-0.008
C4	-0.004	-0.003
O3	0.009	0.008

For the exploration of magnetic exchange mechanism, DFT calculation of **1** base on GGA+U algorithm was conducted by the help of VASP²⁷ program. Effective Hubbard U_{eff} of 6.01 eV for Mn(II) was determined by linear response method of PWSCF program²⁸ (see ESI). Based on optimised geometry with or without the U_{eff} , total DOS (TDOS) and PDOS of linking carboxylate (such as O2, C4 O3 atoms) and Mn(II) ions under the U_{eff} of 0.0 eV and 6.01 eV were calculated, as shown in Fig. 6. In nature, magnetic property is controlled by DOS near Fermi level. A glance at DOS shows the distinct areas between spin-up and spin-down are distributed on the vicinity of Fermi level. TDOS, $3d$ PDOS of Mn(II) and $2p$ PDOS of linking carboxylate are split clearly, resulting in an ordered spin distribution by the exchange interaction. Combining DOS and spin magnetic moment (see Table 1), it is found that magnetic property of **1** is originated from Mn(II) ions and linking carboxylate. Obviously,

anti-ferromagnetic coupling of **1** is derived from 3d electrons of Mn(II) ion propagating by four $-/+$ spin nets of O2–C4–O3. In addition, stronger correlation of Mn(II) ions can effectively affect electronic structure and magnetic property of **1**. There are three aspects, as follows: 1) For Mn(II) and bridging atoms, the spin up (black) PDOS peaks at Fermi level play an dominant roles under the U_{eff} of 0.0 eV, while the spin-down (red) PDOS peaks under the U_{eff} of 6.01 eV are higher than spin-up PDOS peaks. 2) With the value of U_{eff} increasing, the absolute spin magnetic moments of Mn(II) ions enhances (4.72 and $-4.720 \mu_{\text{B}}$ for 6.01 eV, 1.063 and $-1.067 \mu_{\text{B}}$ for 0.00 eV), where the absolute spin magnetic moments of Mn(II) ($4.72 \mu_{\text{B}}$) very approximate to experimental value ($4.94 \mu_{\text{B}}$) at room temperature. 3) The obtained band gap at the U_{eff} of 6.01 eV is larger than that for the U_{eff} of 0.00 eV. Generally, magnetic property of **1** can be attributed to the coupling of paramagnetic Mn(II) ions by $-/+$ spin nets of O2–C4–O3.

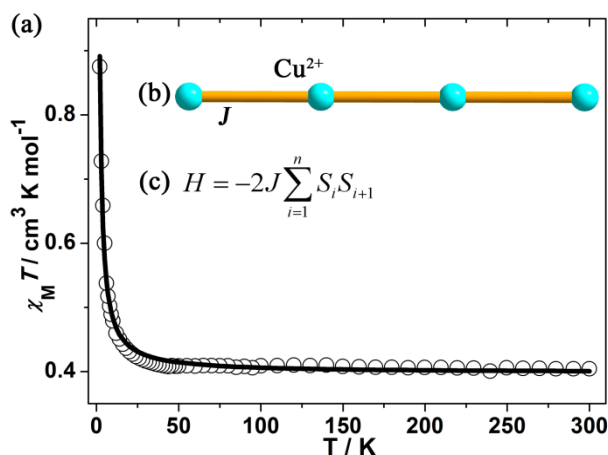


Fig. 7 Experiment plot (black \circ) and QMC fitting line (solid line) of $\chi_{\text{M}}T$ vs T in **4**(a); The sketch of Cu^{2+} distribution (b) and Hamilton operator (c) of **4**;

Likewise, magnetic property of **4** was also measured. The obtained plot of $\chi_{\text{M}}T$ vs T was presented in Fig. 7. The $\chi_{\text{M}}T$ value at room temperature is $0.40 \text{ cm}^3 \text{ mol}^{-1} \text{ K}$, which is in line with the value of $0.375 \text{ cm}^3 \text{ mol}^{-1} \text{ K}$ of single Cu(II) ion following Curie law. Before 50 K, the $\chi_{\text{M}}T$ value almost keeps invariable. Afterward, as the temperature decreasing, the $\chi_{\text{M}}T$ value rapidly increases and reaches a maximum of $0.87 \text{ cm}^3 \text{ mol}^{-1} \text{ K}$ at 2 K. Therefore, it is found that **4** exhibits ferromagnetic property. Furthermore, following Curie-Weiss law²³, the fitting for χ_{M}^{-1} vs T over the temperature range of 100–300 K generates the parameters with $C = 0.39 \text{ cm}^3 \text{ mol}^{-1} \text{ K}$ and $\theta = 3.82 \text{ K}$, as displayed in Fig. S7. The positive Curie temperature validates the ferromagnetic property of **4**. Similarly, QMC fitting was performed (see ESI). In the fitting process, the parameter J was represented as coupling interaction between two Cu(II) ions (see Fig. 7 (b) and (c)), and zJ parameter was invoked to describe the weak interaction between metal-bound chains, *e.g.* Van der Waals' force. The resulting best parameters are that: $J = 2.23 \text{ cm}^{-1}$, $zJ = -0.41 \text{ cm}^{-1}$, $g = 2.06$ and $R = 3.23 \times 10^{-4}$. The 2.23 cm^{-1} value of coupling parameter reveals **4** have weak ferromagnetic property. Negative zJ (-0.41 cm^{-1}) suggests the existence of weak antiferromagnetic interaction between $\{\text{Cu}(\text{COO})\}_n$ chains.

Magnetic propagating mechanism was further identified by DFT calculations. By using linear response method, the U_{eff} of Cu(II) in **4** is 1.68 eV (see ESI). It is evident from Fig. 8 and

Table 2 that the effective Hubbard U_{eff} cannot effectively affect the characteristic of DOS and absolute value of spin magnetic moments, except the change of spin direction. To examine PDOS of Cu(II) ion and linking carboxylate in the neighborhood of Fermi level is very helpful to understand magnetic coupling mechanism. According to PDOS distribution in the U_{eff} of 1.68 eV, it is observed that the main origin of magnetic property in **4** is provided by Cu(II) ions. However, linking carboxylate atoms also contribute spin magnetic moments, see Table 2. Furthermore, we can see that PDOS of d electrons of Cu(II) ions and p electrons of

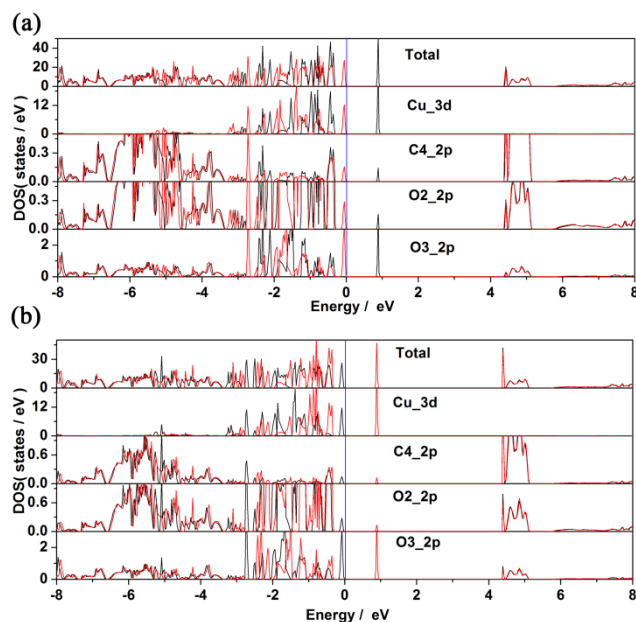


Fig. 8 PDOS of **4** under the U_{eff} of 0.0 eV (a) and 1.68 eV (b) in spin-up (black) and spin-down (red) with Fermi level (blue line).

Table 2 theoretical spin magnetic moments (μ_{B}) of **4**.

$U_{\text{eff}}/ \text{eV}$	0.00	1.68
Cu1	-0.596	0.601
Cu2	-0.596	0.601
O2	-0.002	0.002
C4	-0.009	0.009
O3	-0.072	0.071

linking carboxylate (*e.g.* O2, C4 and O3) have similar peaks, which suggests that these orbitals take part in hybridization. The phenomena play an pivotal role in the indirect propagation between Cu(II) ions of two units, implying that linking carboxylate atoms serve as superexchange pathways. Therefore, ferromagnetic exchanges of two Cu(II) ions come from the spin polarization effect through carboxylate bridge in the $+/+$ spin nets of O2–C4–O3.

Luminescence-structure relation: UV-vis absorption, luminescence spectra and DFT calculation

Solid UV-vis absorption and fluorescence emission spectra of compound **5** were also measured at room temperature. As shown in Fig. 9(a) and (b), two absorption peaks appear at 250 and 375 nm, respectively, while one emission peak at 390 nm was found under the excitation at 250 nm. Previous experimental studies advocated the possible emission mechanisms of Ag(I)-based complexes²⁹. However, this detailed theoretical study is very rare. In order to identify the corresponding mechanism, DFT calculations were carried out. The U_{eff} value of 6.52 eV

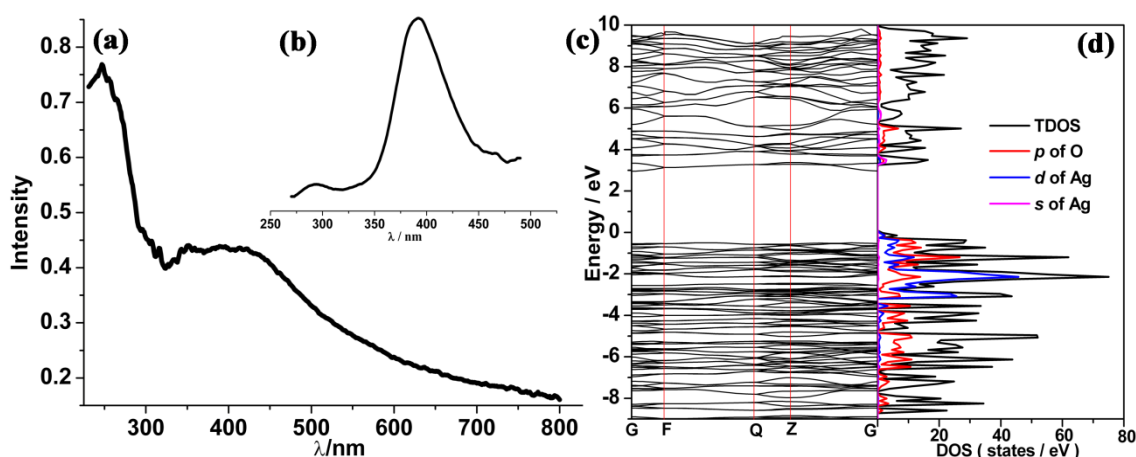


Fig. 9 UV (a), fluorescence spectra (b), band structure (c) and PDOS (d) of **5** with the U_{eff} of 6.52 eV (Fermi level is set to 0.0 eV)

obtained by linear response method (see ESI) was employed to describe strongly correlated interaction of 4d electrons of Ag. Electronic properties (band structure and PDOS) were also examined for relaxed geometry. According to the energy difference between two bands (see Fig. 9(c)), it can be concluded that two absorption peaks (250 and 375 nm) can be attributed to transitions of VB \rightarrow the second empty bands (theoretical value: 302 nm) and VB \rightarrow CB (theoretical value: 381 nm). In comparison with experimental absorption peaks (250 nm), we found that the first transition (VB \rightarrow the second empty bands) plays a dominant role in the UV spectra. Furthermore, an inspection of DOS shows that VB mainly involves in 2p state of carboxylate oxygens and 4d states of Ag, while CB are occupied by 2p state of carboxylate oxygens and 5s states of Ag. On the other hand, frontier orbital analysis results were presented in Fig. 10. Highest occupied molecular orbital (HOMO) and HOMO-2 are concentrated on $d_{x^2-y^2}$ orbitals of Ag atoms and localized dangling p orbitals of oxygen atoms. Lowest unoccupied molecular orbital (LUMO) is contributed by Ag-Ag metal bond (involves 5s orbitals) and dangling p orbitals of oxygen

atoms, whereas LUMO+2 is equally distributed on π^* C=O bond and localized dangling p orbitals of nitrogen atoms from four PODC²⁻ ligands. Therefore, it is found that UV light absorption would mainly induce the electron transfer from 4d states to 5s states of Ag. The wavelength of absorption peaks obtained theoretically are smaller than those of experimental measure (see Fig. S12), owing to an overall overestimated fault of DFT method. But the whole trends of main absorption peaks are in good agreement with experimental values.

For solid state materials, it is difficult to faultlessly explain detailed mechanism of emission by DFT method. However, via the electronic structure, we can still find that under the exposure to excited light, a majority of electrons readily transfer to the region of second empty band, and successively rebound to CB without any emission, and lastly return to CB with the specific emission of 390 nm. In nature, the observed emission peak can be attributed to the electrons transfer from Ag-Ag metal bond (features 5s type orbitals) to localized 4d orbitals of Ag atoms.

Conclusion

In summary, the synthesis and properties of six peptide-based MOFs (Mn(1), Fe(2), Co(3), Cu(4), Ag(5) and Pb(6)) based on H₂PODC have been discussed. Via experimental measures and theoretical calculation, we demonstrated the relations of magnetism-structure and luminescence-structure. Therefore, our studies are beneficial for the effective synthetic strategy of peptide-based MOFs and provide some helps to understand the relations between properties and structures.

Acknowledgements

This work was supported by the 973 project (2013CB733501) and the National Natural Science Foundation of China (21101137, 21136001, 21176221, 21306169 and 91334013).

Notes and references

^a Institute of Industrial Catalysis, College of Chemical Engineering, Zhejiang University of Technology, Hangzhou, People's Republic of China, 310032. Fax: (+86)571-88871037 Tel: (+86)571-88871037. E-mail: jgw@zjut.edu.cn

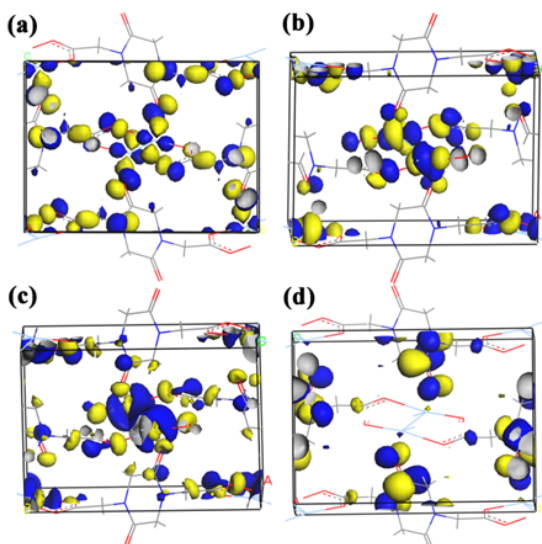


Fig. 10 HOMO-2(a), HOMO(b), LUMO(c) and LUMO+2(d) of compound **5**

^b Center of Modern Experimental Technology, Anhui University, Hefei, People's Republic of China, 230039.

^c Zhejiang Engineering Design Co., Ltd. Hangzhou, People's Republic of China.

[†] Electronic Supplementary Information (ESI) available: [Synthesis and structural information of **1-6**; DFT and QMC computation details; TG, XRD and IR plots; UV-vis theoretical curve]. See DOI: 10.1039/b000000x/

[‡] Footnotes should appear here. These might include comments relevant to but not central to the matter under discussion, limited experimental and spectral data, and crystallographic data.

1. (a) G. B. Gardner, D. Venkataraman, J. S. Moore, S. Lee, *Nature*, 1995, **374**, 792. (b) S. S. Y. Chui, S. M. F. Lo, J. P. H. Charmant, A. G. Orpen, I. D. Williams, *Science*, 1999, **283**, 1148. (c) N. L. Rosi, J. Eckert, M. Eddaoudi, D. T. Vodak, J. Kim, O. M. Yaghi, *Science*, 2003, **300**, 1127. (d) G. Férey, C. Mellot-Draznieks, C. Serre, F. Millange, J. Dutour, S. Surlblé, I. Margiolaki, *Science*, 2005, 2040. (e) X.-J. Kong, L.-S. Long, Z. Zheng, R.-B. Huang, L.-S. Zheng, *Acc. Chem. Res.* 2010, **43**, 201. (f) X.-J. Kong, Y.-P. Ren, L.-S. Long, Z. Zheng, R.-B. Huang, L.-S. Zheng, *J. Am. Chem. Soc.*, 2007, **129**, 7016. (g) X.-J. Kong, Y. Wu, L.-S. Long, L.-S. Zheng, Z. Zheng, *J. Am. Chem. Soc.*, 2009, **131**, 6918. (h) D. Zhao, D. J. Timmons, D. Yuan, H.-C. Zhou, *Acc. Chem. Res.*, 2011, **44**, 123. (i) J. Y. Zou, W. Shi, H. L. Gao, J. Z. Cui, P. Cheng, *Inorg. Chem. Front.*, 2014, **1**, 242.
2. (a) R. Matsuda, R. Kitaura, S. Kitagawa, Y. Kubota, R. V. Belosludov, T. C. Kobayashi, H. Sakamoto, H. Chiba, M. Takata, Y. Kawazoe, Y. Mita, *Nature*, 2005, **436**, 238. (b) H. Furukawa, N. Ko; Y. B. Go, N. Aratani, S. B. Choi, E. Choi, A. Ö. Yazaydin, R. Q. Snurr, M. O'Keeffe, J. Kim, O. M. Yaghi, *Science*, 2010, **329**, 424. (c) S. H. Yang, X. Lin, W. Lewis, M. Suyetin, E. Bichoutskaia, P. J. Parker, C. C. Tang, D. R. Allan, P. J. Rizkallah, P. Hubberstey, N. R. Champness, K. M. Thomas, A. J. Blake, M. Schröder, *Nat. Mater.*, 2012, **11**, 710.
3. (a) J. B. Lin, J. P. Zhang, X. M. Chen, *J. Am. Chem. Soc.*, 2010, 132, 6654. (b) E. D. Bloch, W. L. Queen, R. Krishna, J. M. Zadrozny, C. M. Brown, J. R. Long, *Science*, 2012, **335**, 1606.
4. (a) J. Y. Lee, O. K. Farha, J. Roberts, K. A. Scheidt, S. T. Nguyen, J. Y. Hupp, *Chem. Soc. Rev.*, 2009, **38**, 1450. (b) M. Yoon, R. Srirambalaji, K. Kim, *Chem. Rev.*, 2012, **112**, 1196.
5. (a) M. D. Allendorf, C. A. Bauer, R. K. Bhakta, R. J. T. Houk, *Chem. Soc. Rev.*, 2009, **38**, 1330. (b) Y. J. Cui, Y. F. Yue, G. D. Qian, B. L. Chen, *Chem. Rev.*, 2012, **112**, 1126.
6. M. Kurmoo, *Chem. Soc. Rev.*, 2009, **38**, 1353.
7. C. Wang, T. Zhang, W. B. Lin, *Chem. Rev.*, 2012, **112**, 1084.
8. M. Eddaoudi, D. B. Moler, H.L. Li, B. L. Chen, T. M. Reineke, M. O'keeffe, O. M. Yaghi, *Acc. Chem. Res.*, 2001, **34**, 319.
9. (a) M. Eddaoudi, J. Kim, N. Rosi, D. Vodak, J. Wachter, M. O'Keeffe, O. M. Yaghi, *Science*, 2002, **295**, 469. (b) C. A. Bauer, T. V. Timofeeva, T. B. Settersten, B. D. Patterson, V. H. Liu, B. A. Simmons, M. D. Allendorf, *J. Am. Chem. Soc.*, 2007, **129**, 7136.
10. K. S. Park, A. Ni, A. P. Côté, J. Y. Choi, R. Huang, F. J. Uribe-Romo, H. K. Chae, M. O'Keeffe, O. M. Yaghi, *Proc. Natl. Acad. Sci.*, 2006, **103**, 10186.
11. (a) B. F. Abrahams, M. J. Grannas, T. A. Hudson, R. Robson, *Angew. Chem. Int. Ed.*, 2010, **49**, 1087. (b) S. C. Sahoo, T. Kundu, R. Banerjee, *J. Am. Chem. Soc.*, 2011, **133**, 17950. (c) B. Zhou, A. Kobayashi, H. B. Cui, L. S. Long, H. Fujimori, H. Kobayashi, *J. Am. Chem. Soc.*, 2011, **133**, 5736.
12. (a) R. Vaidyanathan, D. Bradshaw, J.-N. Rebilly, J. P. Barrio, J. A. Gould, N. G. Berry, M. J. Rosseinsky, *Angew. Chem. Int. Ed.*, 2006, **45**, 6495. (b) J. Perez Barrio, J.-N. Rebilly, B. Carter, D. Bradshaw, J. Bacsá, A. Ganin, H. Park, A. Trewin, R. Vaidyanathan, A. Cooper, J. E. Warren, M. J. Rosseinsky, *Chem. Eur. J.*, 2008, **14**, 4521. (c) J. An, S. J. Geib, N. L. Rosi, *J. Am. Chem. Soc.*, 2009, **131**, 8376; (d) J. An, O. K. Farha, J. T. Hupp, E. Pohl, J. I. Yeh, N. L. Rosi, *Nat. Commun.*, 2012, **3**, 604.
13. A. Mantion, L. Massüger, P. Rabu, C. Palivan, L. B. McCusker, A. Taubert, *J. Am. Chem. Soc.*, 2008, **130**, 2517.
14. (a) J. Rabone, Y. F. Yue, S. Y. Chong, K. C. Stylianou, J. Bacsá, D. Bradshaw, G. R. Darling, N. G. Berry, Y. Z. Khimyak, A. Y. Ganin, P. Wiper, J. B. Claridge, M. J. Rosseinsky, *Science*, 2010, **329**, 1053. (b) C. Martí-Gastaldo, J. E. Warren, K. C. Stylianou, N. L. O. Flack, M. J. Rosseinsky, *Angew. Chem. Int. Ed.*, 2012, **51**, 11044. (c) H. Y. Lee, J. W. Kampf, K. S. Park, E. N. G. Marsh, *Cryst. Growth Des.*, 2008, **8**, 296. (d) L. Lang, R. Yu, W. B. Yang, X. Y. Wu, C. Z. Lu, *Cryst. Growth Des.*, 2012, **12**, 3304. (e) W. L. Chen, W. X. Chen, G. L. Zhuang, J. Zheng, L. Tan, X. Zhong, J. G. Wang, *CrystEngComm*, 2013, **15**, 5545. (f) X. J. Kong, G. L. Zhuang, Y. P. Ren, L. S. Long, R. B. Huang, L. S. Zheng, *Dalton Trans.*, 2009, 1707. (g) G. L. Zhuang, X. J. Kong, L. S. Long, R. B. Huang, L. S. Zheng, *CrystEngComm*, 2010, **12**, 2691.
15. (a) T. Sagara, J. Klassen, E. Ganz, *J. Chem. Phys.*, 2004, **121**, 12543. (b) Q. Y. Yang, C. L. Zhong, *J. Phys. Chem. B*, 2006, **110**, 655. (c) F. Salles, A. Ghoufi, G. Maurin, R.G. Bell, C. Mellot-Draznieks, G. Férey, *Angew. Chem. Int. Ed.*, 2008, **47**, 8487. (d) T. Mueller, G. Ceder, *J. Phys. Chem. B*, 2005, **109**, 17974. (e) K. Sillar, A. Hofmaan, J. Sauer, *J. Am. Chem. Soc.*, 2009, **131**, 4143. (f) L. Grajciar, O. Bludsky, P. Nachtigall, *J. Phys. Chem. Lett.*, 2010, **1**, 3354.
16. (a) K. Zhang, L. L. Zhang, J. W. Jiang, *J. Phys. Chem. C*, 2013, **117**, 25628. (b) H. Frost, T. Duren, R. Q. Snurr, *J. Phys. Chem. B*, 2006, **110**, 9565. (c) V. D. Berg, W. C. Annemieke, C. O. Arean, *Chem. Commun.*, 2008, 668. (d) S. Han, W. A. Goddard, *J. Am. Chem. Soc.*, 2007, **129**, 8422. (e) Y. L. Xiao, Q. Y. Yang, D. H. Liu, C. L. Zhong, *CrystEngComm*, 2013, **15**, 9588. (f) A. Comotti, A. Fraccarollo, S. Bracco, M. Beretta, G. Distefano, M. Cossi, L. Marchese, C. Riccardi, P. Sozzani, *CrystEngComm*, 2013, **15**, 1503.
17. (a) K. S. Walton, A. R. Millward, D. Dubbeldam, H. Frost, J. J. Low, O. M. Yaghi, R. Q. Snurr, *J. Am. Chem. Soc.*, 2008, **130**, 406. (b) A. Vishnyakov, P. Ravikvitch, A. V. Neimark, M. Bulow, Q. M. Wang, *Nano Lett.*, 2003, **3**, 713. (c) Q. T. Ma, Q. Y. Yang, A. Ghoufi, G. Férey, C. L. Zhong, G. Maurin, *Dalton Trans.*, 2012, **41**, 3915. (d) A. Malkick, S. Saha, P. Pachfule, S. Roy, R. Banerjee, *Inorg. Chem.*, 2011, **50**, 1392. (e) K. Zhang, Y. F. Chen, A. Nalaparau, J. W. Jiang, *CrystEngComm*, 2013, **15**, 10358.
18. C. B. Ma, C. N. Chen, Q. T. Liu, *CrystEngComm*, 2005, **7**, 650.
19. V. A. Blatov, *IUCr CompComm Newsletter*, 2006, 7, 4.
20. W. X. Chen, S. T. W. L. S. Long, R. B. Huang, L. S. Zheng, *Cryst. Growth Des.*, 2007, **7**, 1171.
21. L. Brammer, M.D. Burgard, M. D. Eddleston, C. S. Rodger, N. P. Rath, H. Adams, *CrystEngComm*, 2002, **4**, 239.
22. J. X. Yuan, M. L. Hu, A. Morsali, *Inorg. Chem. Commun.*, 2006, **9**, 277.
23. K. Charles, Introduction to solid state physics (7th ed.). 1996.
24. (a) J. M. Herrera, A. Bleuzen, Y. Dromzée, M. Julve, F. Lloret, M. Verdaguer, *Inorg. Chem.*, 2003, **42**, 7052; (b) D. Maspocho, N. Domingo, D. Ruiz-Molina, K. Wurst, J. M. Hernández, G. Vaughan, C. Rovira, F. Lloret, J. Tejada, J. Veciana, *Chem. Commun.*, 2005, 5035.
25. B. Bauer, L.D. Carr, H. G. Evertz, A. Feiguin, *J. Stat. Mech.*, 2011, P05001.
26. C. Mennerich, H. H. Klauss, M. Broekelmann, *Phys. Rev. B*, 2006, **73**, 174415.
27. G. Kresse, J. Hafner, *Phys. Rev. B*, 1993, **48**, 13115.
28. (a) M. Cococcioni, S. de Gironcoli, *Phys. Rev. B* 2005, **71**, 035105; (b) P. Giannozzi, S. Baroni, N. Bonini, M. Calandra, R. Car, et al. *J. Phys.: Condens. Matter*, 2009, **21**, 395502.
29. (a) C. M. Che, S. W. Lai, *Coor. Chem. Rev.*, 2005, **249**, 1296; (b) T. Ren, C. Lin, P. Amalberti, D. Macikenas, J. D. Protasiewicz, J. Clayton Baum, T. L. Gibson, *Inorg. Chem. Commun.*, 1998, **1**, 23. (c) J. H. Yang, S. L. Zheng, X. L. Yu, X. M. Chen, *Cryst. Growth Des.*, 2004, **4**, 831.